

A Model of the Magnetic Fields Created by Single Motor Unit Compound Action Potentials in Skeletal Muscle

Kevin Kit Parker and John P. Wikswo, Jr.,* *Member, IEEE*

Abstract—We have developed a computationally simple model for calculating the magnetic-field strength at a point due to a single motor unit compound action potential (SMUCAP). The motor unit is defined only in terms of its anatomical features, and the SMUCAP is approximated using the tripole model. The distributed current density J is calculated within the volume defined by the motor unit. The law of Biot and Savart can then be cast in a form necessitating that J be integrated only over the region containing current sources or conductivity boundaries. The magnetic-field strength is defined as the summation of the contributions to the field made by every muscle fiber in the motor unit. Applying this model to SMUCAP measurements obtained using a high-resolution Super Conducting Quantum Interference Device (SQUID) magnetometer may yield information regarding the distribution of action currents (AC's) and the anatomical properties of single motor units within a muscle bundle.

Index Terms—Electromyogram, magnetomyogram, mathematical model, SQUID.

I. INTRODUCTION

THE electroneurogram (ENG) and the electromyogram (EMG) are recordings of an electric potential difference between two points in the vicinity of an active nerve or muscle bundle. The measurements can be made using surface electrodes on the skin over the active bundle, or with invasive electrodes in or around the bundle. Ionic currents propagating along the length of fibers in the bundle give rise to action potentials (AP's) which are manifest as the electric potential difference between the electrodes. These currents also produce the magnetic fields that are recorded as the magnetoneurogram (MNG) and the magnetomyogram (MMG). These signals may be defined as the measurement of one component of the magnetic field versus time, where the sources of the field are the propagating action currents (AC's). For bundles where multiple fibers are active at the same time and contribute to the measured signal, the summation of these signals is defined as a compound signal, i.e., the action field (AF) measured from a muscle bundle where multiple fibers are active is referred to as the compound action field (CAF).

Manuscript received August 11, 1995; revised May 6, 1997. This work was supported in part by the National Institutes of Health under Grants NS 24751 and NS 19794. *Asterisk indicates corresponding author.*

K. K. Parker is with the Living State Physics Group, Department of Physics and Astronomy, Vanderbilt University, Nashville, TN 37235 USA.

*J. P. Wikswo, Jr. is with the Living State Physics Group, Department of Physics and Astronomy, Vanderbilt University, Box 1807 Station B, Nashville, TN 37235 USA (e-mail: wikswojp@ctrvax.vanderbilt.edu).

Publisher Item Identifier S 0018-9294(97)06900-0.

Of particular interest is the MMG, although much of what we state about the MMG is applicable to the MNG in the appropriate context. The EMG and the MMG have similarities, as they are both measurements of the same phenomena of propagation of action signals along an excitable fiber, that are documented in the literature [1], [2]. Recordings made in our laboratory on single motor units (SMU's) of the extensor digitorum longus in rats [1] and a subsequent analysis of the magnetic recording technique [3] showed two important features of the MMG: the AF was less sensitive to the position of the magnetometer than the electric potential recording was to electrode placement, and the AF associated with AC in cylindrical fibers is less sensitive to the conductivities of the medium surrounding the bundle than is the surface electric potential. Thus, magnetic recordings should provide a clearer immediate picture of the bundle physiology than do the extracellular electric signals recorded on the skin.

The MMG offers several additional advantages over the EMG. The noninvasive nature of the MMG is clinically attractive over needle electrode recordings of the EMG and possibly more reliable than surface recorded electrodes [4]. Electrode measurements are greatly affected by the surrounding tissue, whose conductivities can vary by orders of magnitude [5]. The MMG does not show this sensitivity because the magnetic permeability of all biological tissues is very close to that of free space.

Yet another advantage of the MMG over the EMG arises from the vector nature of the magnetic field. All three components of the magnetic-field vector may be measured with the same ease as can a single component. The surface-recorded EMG is restricted to the plane of the skin and yields no such vector information. Such vector information could aid in the localization of the bioelectric source(s). It is important to note, however, that the magnetic field outside the body can be described by a scalar magnetic potential, so a complete map of a single field component would contain all of the information present in the magnetic field.

Previous models of the MMG have been computationally exhaustive [6]. We have developed a simple model of a single, cylindrical fiber in an unbounded, homogeneous conductor to support inverse techniques capable of determining the position of the effective electrical axis of a motor unit and the number of fibers in the motor unit [7], [8]. Thus, we have reduced the description of the motor unit in the forward model to anatomical features and other features based on single fiber

recordings in the laboratory environment. In this paper, we first develop a model of the extracellular potential based on our assumption regarding the nature of the transmembrane potential and then we develop a model of the magnetic fields produced by the intracellular currents. Simulations with this model indicate that the model is an accurate representation of the physiological phenomena we have observed.

II. A MODEL OF THE SINGLE MOTOR UNIT COMPOUND ACTION POTENTIAL (SMUCAP)

A model of the AP propagating along an excitable fiber was introduced by Plonsey [9], who made assumptions about the transmembrane potential in order to derive the extracellular potential. These assumptions are summarized in Fig. 1, in which the transmembrane is approximated as a triangular waveform, Fig. 1(a), whose first and second spatial derivatives are also shown in Fig. 1(b) and 1(c), respectively. We present the relevant results of Plonsey's model.

We can assume that the propagation of the AP along the length of an excitable fiber is quasi-static, so that the curl of the extracellular electric field is zero and, hence, it can be described as the negative gradient of a scalar potential, Φ_e . In the volume containing the excited fiber, the total current density can be separated into two components

$$\mathbf{J} = \mathbf{J}^i - \sigma_e \vec{\nabla}^2 \Phi_e \quad (1)$$

where \mathbf{J}^i is the impressed current density, which describes the current sources produced by the active fiber, and $\sigma_e \vec{\nabla}^2 \Phi_e$ is the Ohmic-volume current density, i.e., the return current in the medium.

We wish to determine the extracellular potential, Φ_e , given a simplified description of \mathbf{J}^i from an active fiber. In the quasi-static limit, we can neglect displacement currents, so the divergence of the total current density is zero, and (1) becomes

$$\vec{\nabla} \cdot \mathbf{J} = \mathbf{J}^i - \sigma_e \nabla^2 \Phi_e = 0, \quad (2)$$

This is Poisson's equation, which has the solution

$$\Phi_e(r) = -\frac{1}{4\pi\sigma_e} \int_V \frac{\vec{\nabla} \cdot \mathbf{J}^i(\mathbf{r}')}{|\mathbf{r} - \mathbf{r}'|} dV' \quad (3)$$

where \mathbf{r} is the field point at which Φ_e is being measured and \mathbf{r}' is the source point.

We immediately identify $-\vec{\nabla} \cdot \mathbf{J}^i$ as the current source density ρ_e in the extracellular space, i.e., any impressed current density that disappears from the intracellular space must cross the membrane as a current, i_m , and then appear as a current source in the extracellular space.

We now need to relate the current source density to the transmembrane potential, V_m . If we consider the extracellular space to be extensive in comparison to the intracellular space, changes in Φ_e will be much smaller than changes in the intracellular potential, Φ_i and can, to first order, be ignored, i.e., we limit ourselves to the core-conductor model [11]. In this case

$$V_m = \Phi_i - \Phi_e \cong \Phi_i \quad (4)$$

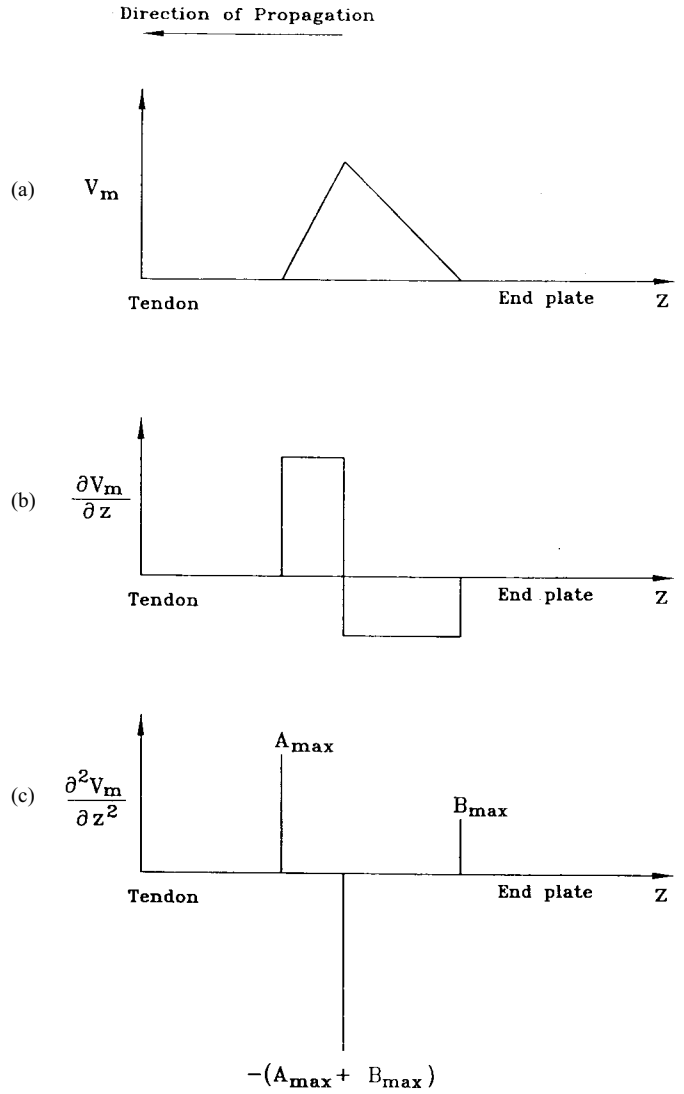


Fig. 1. The tripole model. Propagation is toward the left: (a) the transmembrane potential is approximated as a triangular waveform, (b) the first spatial derivative of the transmembrane potential is equal to the intracellular current, and (c) the second spatial derivative of the transmembrane potential is proportional to the membrane current. (Adapted from [8].)

and the membrane current is given by the continuity condition

$$i_m = \frac{\partial I_i}{\partial z}. \quad (5)$$

Φ_i and the intracellular current, I_i , are related by Ohm's law

$$I_i r_i = -\frac{\partial \Phi_i}{\partial z} \cong \frac{\partial V_m}{\partial z} \quad (6)$$

where r_i is the intracellular resistivity per unit length of the fiber, defined by

$$r_i = \frac{1}{\pi a^2 \sigma_i} \quad (7)$$

where σ_i is the intracellular conductivity and a is the axon radius. The three previous expressions can be combined to yield

$$i_m = \frac{1}{r_i} \frac{\partial^2 \Phi_i}{\partial z^2} \approx \frac{1}{r_i} \frac{\partial^2 V_m}{\partial z^2} \quad (8)$$

which shows that the current flowing outward from the membrane element dz is directly proportional to the second spatial derivative of the transmembrane potential.

Because we are using the triangular AP in Fig. 1(a), $\partial^2 V_m / \partial z^2$ is nonzero only at three points, as shown in Fig. 1(c), and the current source density is given by

$$\rho_e(z') = \sum_{k=1}^N i_k \delta(z - z') \quad (9)$$

where i_k and z_k are the strength and location, respectively, of the k th current source and $\delta(z - z')$ is the Dirac delta function [10]. We then rewrite the volume integral of (3) as

$$\Phi_e(r) = \frac{1}{4\pi\sigma_e} \sum_{k=1}^N \int_V \frac{i_k \delta(z - z')}{|\mathbf{r} - \mathbf{r}'|} dV'. \quad (10)$$

Because of the delta functions, the integral reduces to a sum of the three sources, and the extracellular potential is given by

$$\Phi_e(r) = \frac{a^2 \sigma_i}{4\sigma_e} \left(\frac{A_{\max}}{|\mathbf{r} - \mathbf{r}'_1|} - \frac{A_{\max} + B_{\max}}{|\mathbf{r} - \mathbf{r}'_2|} + \frac{B_{\max}}{|\mathbf{r} - \mathbf{r}'_3|} \right) \quad (11)$$

where A_{\max} and B_{\max} are the source strengths determined by the shape of the AP as depicted in Fig. 1(c).

To summarize Plonsey's model, if the transmembrane potential is approximated as a triangular waveform, the extracellular potential may be described as being due to a tripole whose spatial and temporal extent matches that of the transmembrane potential. The tripole can be viewed as the combination of two bipoles (A_{\max} and $-A_{\max}$) and ($-B_{\max}$ and B_{\max}) whose pole strengths sum to zero.

III. THE CURRENT ELEMENT MODEL OF THE MAGNETIC ACTION FIELD

Given the pair of tripoles, we must now determine the magnetic field that they produce. The magnetic field from a current density \mathbf{J} is given by the law of Biot and Savart, which can be written as

$$\mathbf{B}(\mathbf{r}) = \frac{\mu_o}{4\pi} \int_V \frac{\vec{\nabla} \times \mathbf{J}(\mathbf{r}')}{|\mathbf{r} - \mathbf{r}'|^3} d^3 r'. \quad (12)$$

Because the Ohmic currents in a homogeneous unbounded medium have no curl, the extracellular currents in the volume outside the fiber do not contribute to the magnetic field. The membrane currents do not contribute significantly to the magnetic field [15]. As a result, the remaining contributions to the curl of \mathbf{J} in (12) is the discontinuity in the axial intracellular and extracellular AC's at the membrane. Because the extracellular current density is so much lower, the dominant contribution to \mathbf{J}^i is the discontinuity in intracellular current. Since this current is assumed to be axial and uniform within the fiber, the volume integral of (13) may be rewritten as a line integral

$$\mathbf{B}(\mathbf{r}) = \frac{\mu_o}{4\pi} \int_l \frac{I_i d\mathbf{l} \times (\mathbf{r} - \mathbf{r}')}{|\mathbf{r} - \mathbf{r}'|^3}. \quad (13)$$

This integral can be divided into two parts, one for the depolarization phase and the other for repolarization, and the spatial extent of each phase determines the limits of integration. Combining this with (6), we have

$$\mathbf{B}(\mathbf{r}) = \frac{\mu_o}{4\pi} \frac{1}{r_i} \left[\int_{z_1}^{z_2} \frac{\left(\frac{\partial V_m}{\partial z} \right) d\mathbf{z}' \times (\mathbf{r} - \mathbf{r}')}{|\mathbf{r} - \mathbf{r}'|^3} + \int_{z_2}^{z_3} \frac{\left(\frac{\partial V_m}{\partial z} \right) d\mathbf{z}' \times (\mathbf{r} - \mathbf{r}')}{|\mathbf{r} - \mathbf{r}'|^3} \right]. \quad (14)$$

For the simple $V_m(t)$ in our model, (14) can be solved analytically and, hence, is computationally simple and efficient, in contrast to the Gaussian or Bessel function series used in other models [6], [15].

IV. PROPAGATION MECHANISMS

The stationary model presented so far for the AP does not yet completely describe the electrical activity of an actual muscle bundle. For multiple fibers, such as those that comprise an SMU, the expressions in either (11) for the AP or (14) for the AF can be summed over the fibers in the motor unit. However, the model must be adapted to account for the initiation of the AS at the motor endplate and the termination of the AS upon its arrival at the tendon.

Plonsey's model of the AP was adapted to the problem of the SMUAP by McGill and Huynh [12]. McGill [13] then developed a mechanism to account for the initiation of the AP at the motor endplate region and its termination at the tendon. This mechanism will be discussed in terms of the model of the AP and then will be adapted to the current-element model.

A. Initiation and Termination of a Single Fiber AP

In McGill's model of AP initiation, at a time t_o , an AS propagating along a motor neuron reaches the motor endplate region of a muscle fiber. This triggers an AS in the muscle fiber that will propagate in both directions along the length of the muscle fiber away from the motor endplate region. Thus, at t_o , two sources appear at the motor endplate and immediately begin to propagate away from the endplate in opposite directions. This is followed by the appearance of two sinks at the endplate region, which then move away from the endplate in a similar fashion. Finally, two more sources appear and move away from the endplate, completing the tripole. This process is depicted in Fig. 2. When both two-sources/one-sink combinations are fully created and in motion, each set propagates away from the motor endplate region and toward the tendon at the end of the fiber.

Upon arrival at the end of the fiber under consideration, the first source comes to a halt and remains there. Subsequently, the stronger sink arrives at the tendon canceling the first source and leaving a net sink. Finally, the last sources arrive at the ends of the fiber so that all sources and sinks then sum to zero, extinguishing the AP. To account for the contributions

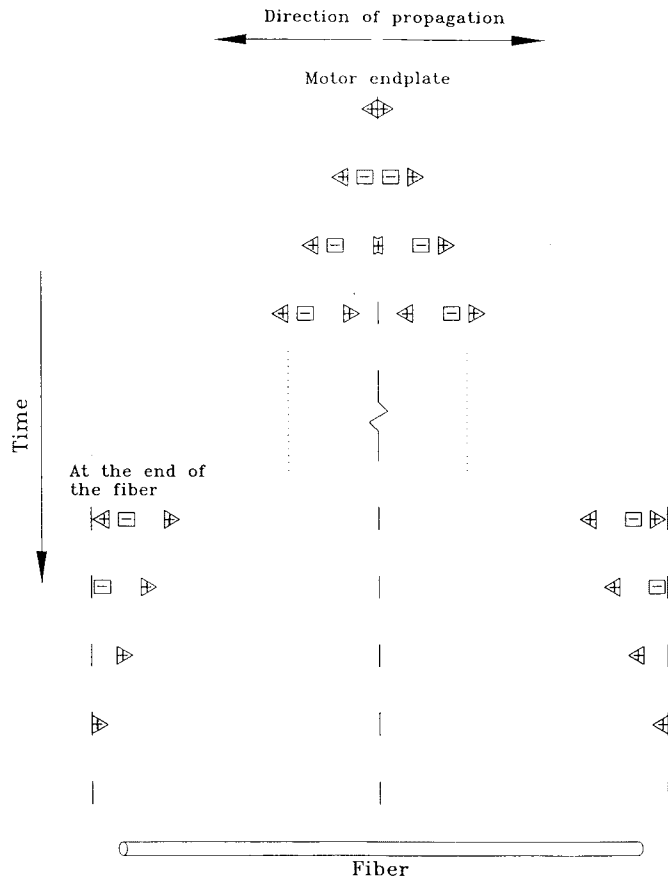


Fig. 2. Propagation in the tripole model of the SMUCAP. Poles depart from the motor endplate region one at a time, until two tripoles [Fig. 1(c)] are propagating in either direction toward the tendons on either end of the muscle fiber. Upon arrival at the tendon, the poles accumulate and sum to zero, extinguishing the AP.

of both source/sink sets propagating along the length of the fiber, (11) is summed over the various sources and sinks that are propagating in either direction along the length of the fiber to obtain the single fiber AP, and then again over the number of fibers in the motor unit to yield the single motor unit compound action potential (SMUCAP).

B. Initiation and Termination of the Action Field

We introduce a similar method by which the current-element pairs in the current-element model of the single motor unit action field (SMUCAF) are launched from the motor endplate region, and eventually collapse at the junction with the tendons on either side of the muscle fiber. Rather than launching poles from the motor endplate region, though, the current elements are created and launched so that the AF will have the same spatial extent and duration as the AP. This process is depicted in Fig. 3. In contrast to the sudden appearance or disappearance of the poles, the length of each current element increases or decreases in time until the current element is either fully established or completely disappears. In the simplest, far-field approximation, the strength of the magnetic field is proportional to the length of the current element and, hence, this process is central to the time dependence of the magnetic fields.

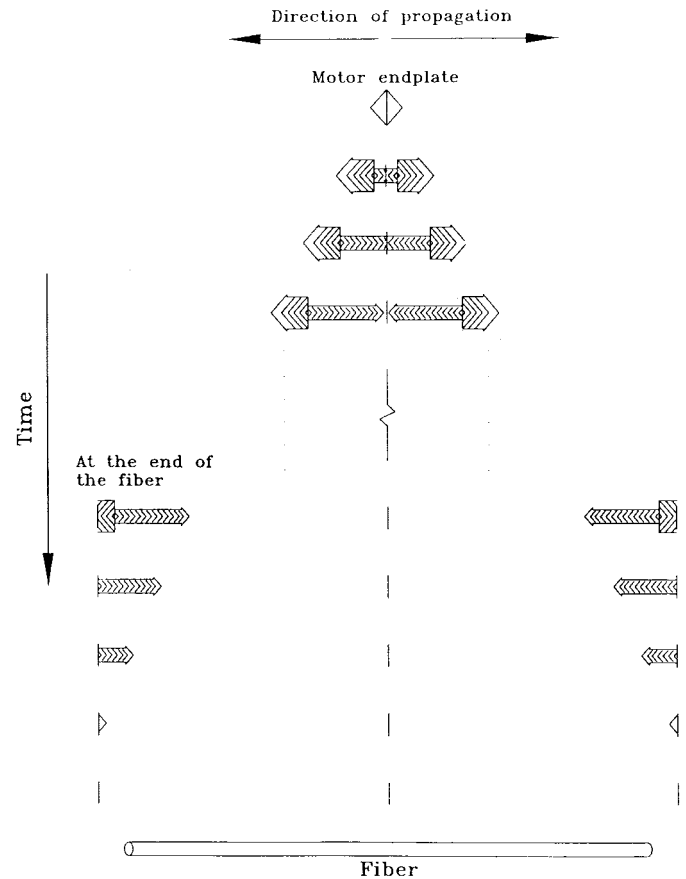


Fig. 3. The current element model of the SMUCAF. Current elements form at the motor endplate region, until two pairs of current elements [Fig. 1(b)] propagate toward the tendons on either side of the muscle fiber. Upon reaching the tendon, the current elements collapse, extinguishing the AF.

These two models are explained in terms of appearance times. For the tripole model, these appearance times correspond to the departure of poles from the motor endplate region. For the current-element model, these times correspond to the departure of the ends of current elements with finite, yet variable, length from the motor endplate region. Thus, the position of either the pole or the end of the current element along the length of the fiber at any time during the course of a simulation is calculated as a function of the conduction velocity, its appearance time, and the location of the motor endplate region along the fiber's length.

For $t \leq h(k)$, where $h(k)$ is the appearance time for the k th pole or current-element end, the location of a pole or current-element end is given by

$$z_k(t) = \lambda + e_k u(t - h_k) \tag{15}$$

for $t \leq (h(k) - (L - e(k)\lambda)/u)$, where u is the conduction velocity, $e(k)$ is a positive or negative value, depending upon which direction along the length of the fiber the k th pole or current element propagates, and λ is the length of the motor endplate region. Prior to the appearance time, the poles exist at the endplate location. The pole or current-element end has arrived at the tendon when

$$z_k(t) = e_k L \tag{16}$$

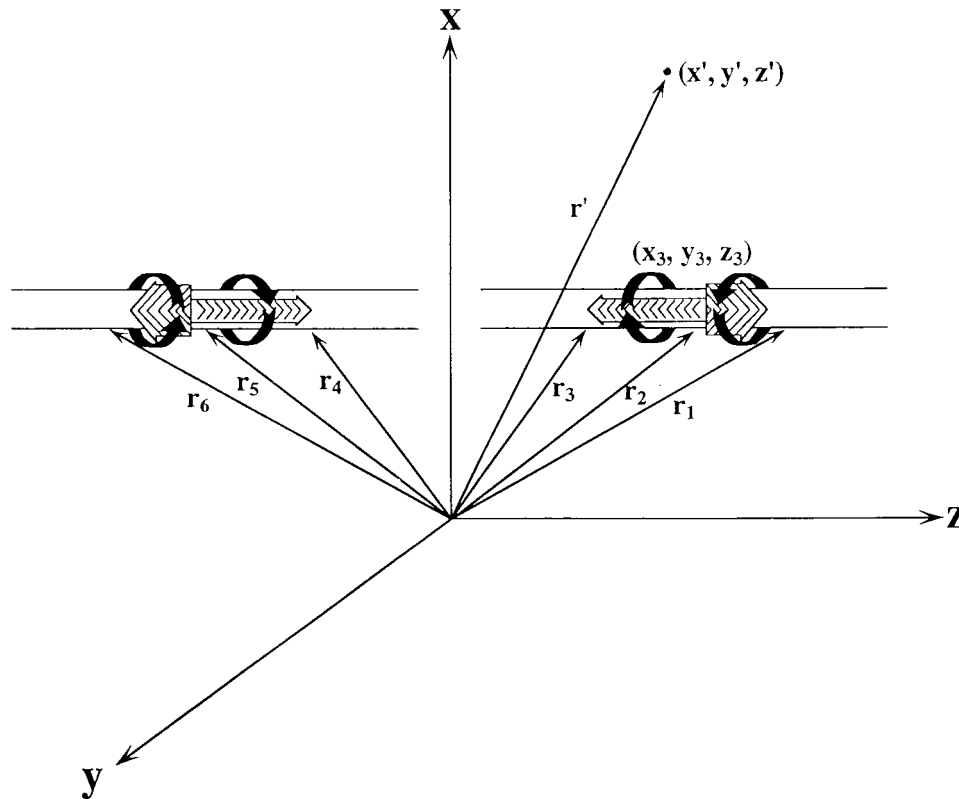


Fig. 4. A single fiber is depicted with its motor endplate region at the origin of the x -axis. At the field point x', y', z' , the field strength is calculated as the sum of the contributions of the current element pairs propagating in either half of the fiber.

where L is the distance from the motor endplate region to the tendon.

Thus, the method of propagation in our model is defined by departure times from the endplate region. These departure times correspond to the formation of sources and sinks in the model of the SMUCAP and the creation of current elements in the model of the SMUCAF. The departure times, in conjunction with the propagation velocity, determine the spatial and temporal extent of the signal. We depict the simulated experimental situation in Fig. 4, where the AP is propagating away from the motor endplate in opposite directions along the single fiber, and the SMUCAF is measured at point (x', y', z') .

V. RESULTS OF SIMULATIONS

We tested the model using a computer simulation written in FORTRAN on a VAX 8800 computer. For all of the simulation results presented, the fiber(s) lie along the z -axis, and propagation of the action signal occurs in both directions along the z -axis. In all cases except the multifiber simulation, the endplate was assumed to be located at the middle of the fiber, i.e., at $z = 0.0$. The parameter values for all single-fiber simulation results are given in Table I.

A. Biphasic Action Field and Propagation

Fig. 5(a), an experimental result reported by van Egeraat *et al.* [14], shows the axial AC in a single muscle fiber from the gastrocnemius muscle of the bullfrog (*Rana catesbiana*) as measured by a toroid. In Fig. 5(b), we present the x -

TABLE I
PARAMETER VALUES FOR THE CURRENT-ELEMENT
MODEL OF THE SMUCAF AS SIMULATED IN FIG. 5

Current in First Element	43.3 nA
Current in Second Element	-18.6 nA
Conduction Velocity	3.0 m/s
Fiber Length	20 mm
Number of Fibers	1
Appearance Times	0.0, 0.52, and 1.73 ms
Field Point	$x'=2.0, y'=2.0, z'=5.0$ mm

component of the magnetic field of a single muscle fiber as simulated with the current-element model. The simulated result is biphasic like its experimental counterpart, and we see that each phase corresponds to a current element. Values for the current elements were determined from the experimental data in Fig. 5(a). For the simulation result in Fig. 5(b), the x - and y -coordinates of the field point are the same (2.0 mm in this simulation). When this is the case, the x - and y -components of the field will have the same peak-to-peak amplitude because the field encircles the fiber. As the y -coordinate of the field point approaches the y -coordinate of the fiber, the x -component of the field would disappear, and vice versa for variations in the x -coordinate and the y -component of the field.

We also found for the range of departure times used that the peak-to-peak amplitude of the AF is proportional to the

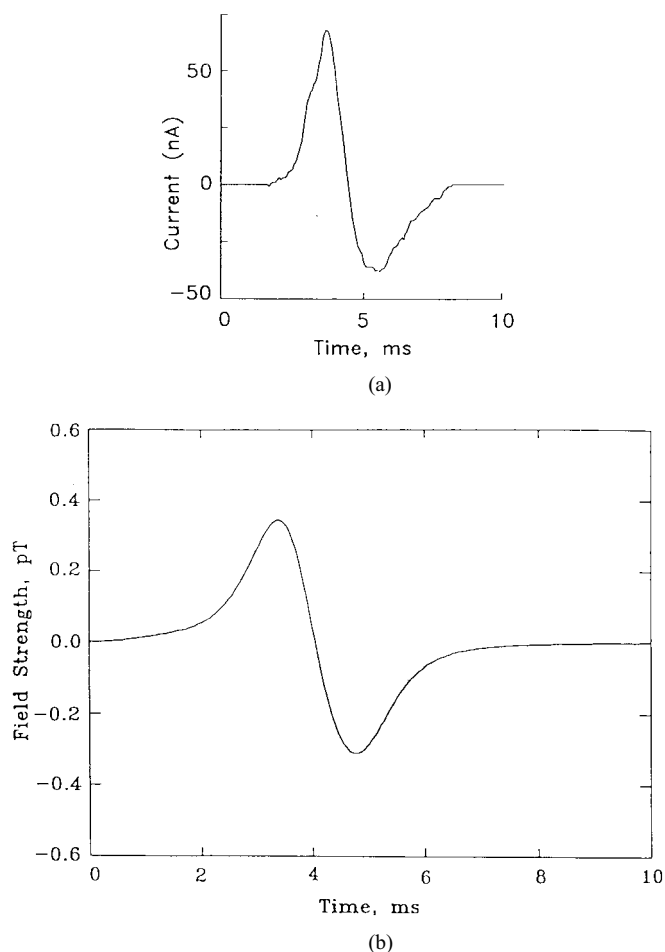


Fig. 5. Comparison of experimental and theoretical results for the magnetically detected AC: (a) AC in a single muscle fiber of a bullfrog gastrocnemius as recorded by a toroid (reprinted from [13] with permission of the Biophysical Society) and (b) simulation of the x component of the magnetic field from a single muscle fiber with the current-element model.

number of fibers in the motor unit, consistent with the results of Wijesinghe's more complex anisotropic model.

In Fig. 6, we see that the peak-to-peak amplitude falls off as $1/r$ within 1 mm of the fiber, as $1/r^2$ between 1 mm and 10 mm from the fiber, and as $1/r^3$ at distances greater than 10 mm away from the fiber, consistent with earlier results [15].

Fig. 7(a)–(j) depicts a simulation of the y -component of the AF from the propagating AC's as would be detected by a SQUID magnetometer that is scanned in a plane 8.0 mm above the motor unit. The surfaces are presented as snapshots 0.5 ms apart, with the first at the instant that the nerve action signal reaches the synaptic region of the muscle fiber. The endplate of the simulated fiber is located at its geometric center. The fibers of the motor unit modeled have a total length of 20 mm, thus, the endplate is located at 0 mm on the z -axis of the surface plots presented. The signal then propagates away from the endplate in both directions at 3 mm/ms. In Fig. 7(a), the positive current elements have emerged from the endplate by 0.5 ms after the initiation of the AP. The signal, recorded at a fixed point, is monophasic, but in time the phases have opposite sign on either side of the motor endplate. The amplitudes of the opposing phases

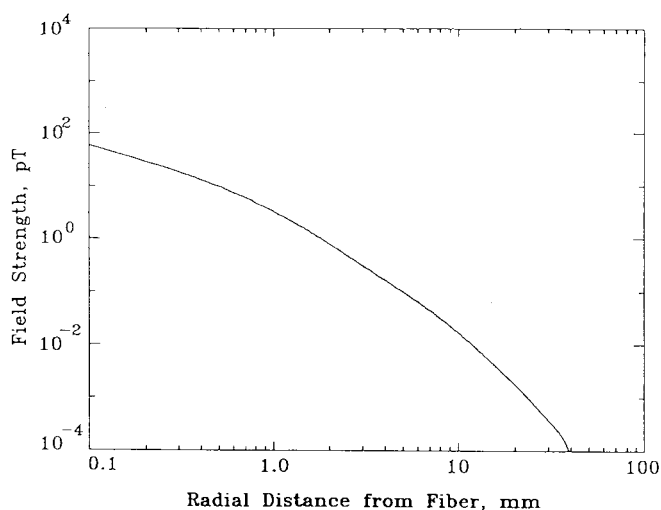


Fig. 6. The radial variation of the peak-to-peak amplitude of the AF. The field falls off as $1/r$ within a 1-mm distance from the fiber, as $1/r^2$ at distances between 1 mm and 10 mm, and as $1/r^3$ at distances greater than 10 mm from the fiber.

are attenuated somewhat by some spatial canceling between the two due to their close proximity. In Fig. 7(b) and 7(c), we see the amplitudes growing as the phases move farther apart and the leading current elements in the two pairs form. In Fig. 7(d), 2 ms after the initiation of the AP at the endplate, the second current elements have emerged from the endplate, but they are not apparent because they are in close proximity to and oppose each other and are dominated by the field of the full leading current elements. In Fig. 7(e), the trailing current elements have emerged fully so that four phases are visible corresponding to the biphasic signals moving along each half-length of the fiber. In Fig. 7(g), the first current elements of the current-element pairs have reached the tendon and collapsed, thus, the two phases seen in the plot represent the two trailing current elements as they propagate toward the tendons at either end of the muscle fiber. In the following sequence, Fig. 7(h)–(j), the fields from these remaining current elements are shown decreasing in amplitude as the elements collapse at their respective tendons. The amplitude of this phase is bigger than previously because there is no cancellation from the leading dipole, which has collapsed at the tendon.

B. Comparison of Experimental and Theoretical Results

Fig. 8(a) and (b) provides a comparison between experimental data [16] and the results from the propagating current-element model. Experimental data was collected by scanning a toroid along a rat extensor digitorum longus (EDL) bundle, from the distal region termination over the endplate region and slightly beyond. The fiber half-length was approximately 10 mm. The endplate region is easily seen as the point where the crossover in polarity occurs, as in the case of the simulated SQUID scans in Fig. 7(a)–(j). The experimental data presented represents the calculated AC's derived from the recorded AF's. In Fig. 8(b), where the field point for magnetic-field calculation is the same as the case in Fig. 5(b) ($2\sqrt{2}$ mm from the idealized motor unit), the strength of the AF grows as the current element emerges from the endplate region, propagates

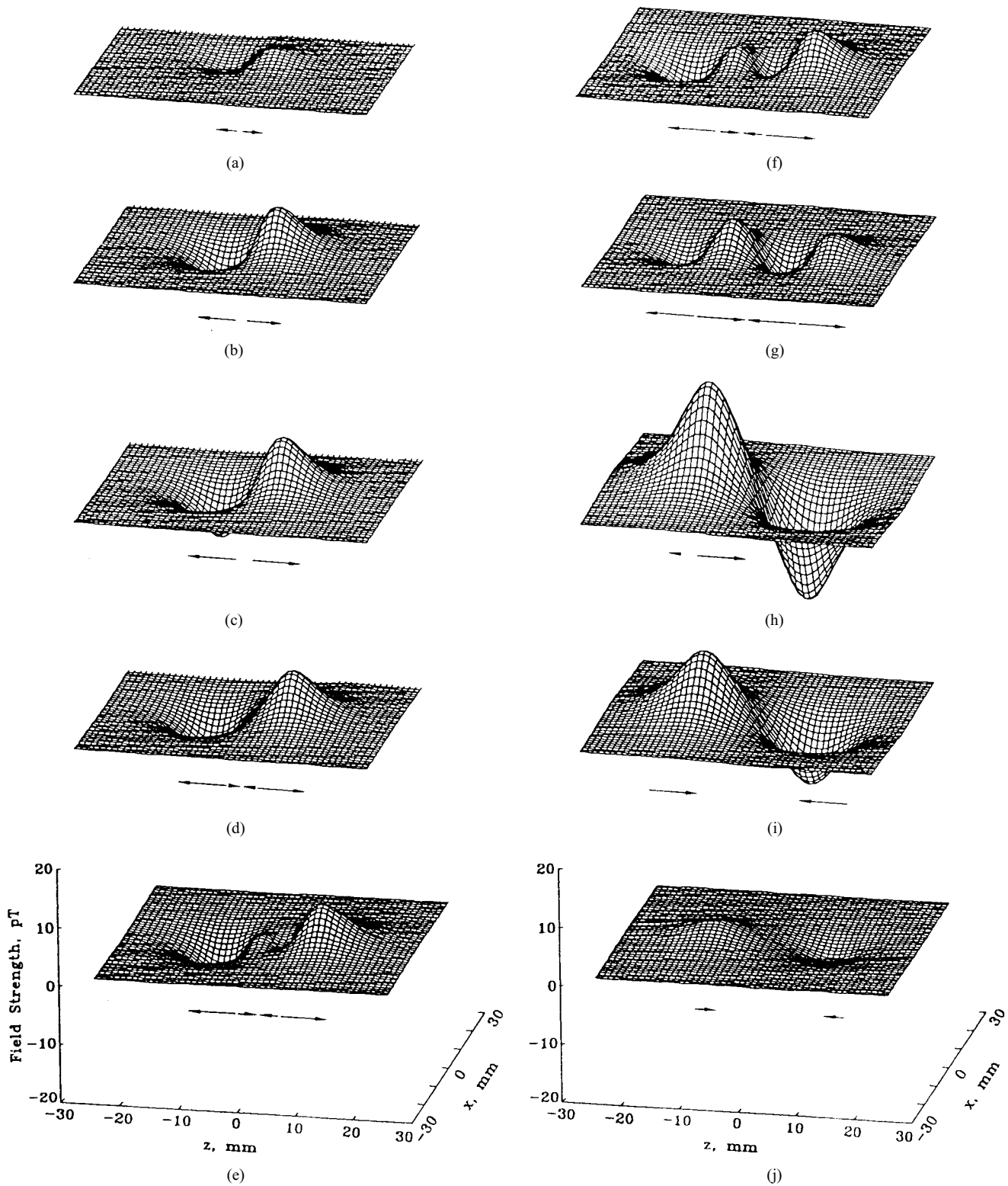


Fig. 7. Simulated scans of the vertical component of the magnetic field over a plane 8 mm above an idealized motor unit. The fiber extends from $z = -10$ to 10 mm. Snapshots are shown in 0.5-ms intervals. For clarity, the line representation of the model is shown beneath it.

along the length of the fiber, and then the amplitude of the positive phase increases quickly as the signal approaches the tendon. As the toroid is scanned beyond the length of the fiber, the field dies off gradually. Fig. 8(b) shows the results of a corresponding simulation with the propagating current-element model. Differences in the experimental and theoretical results

may arise from the complicated geometry of the rat EDL, as compared to the cylindrical symmetry of the propagating current-element model, the fact that our model included only a single fiber in comparison to the several hundred in the rat EDL, and the possibility that the propagation velocity may not be constant as the AC approaches the tendon in the rat EDL.

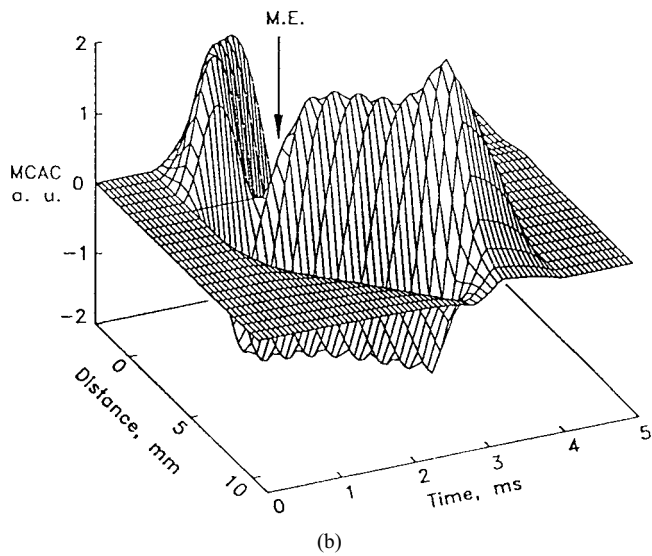
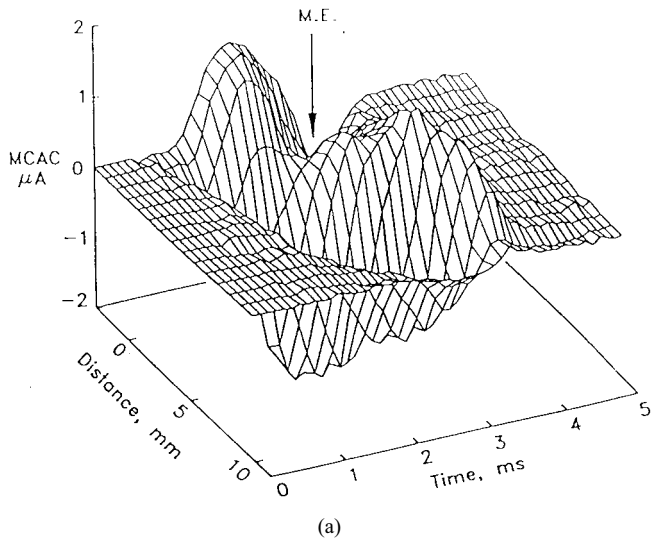


Fig. 8. The temporal and spatial dependence of the muscle compound AC following the stimulation at the motor endplate. (a) The muscle was threaded through the toroid and the toroid was scanned along its length and (b) is a simulated scan of an idealized motor unit with the current-element model of the SMUCAF.

One easily detectable difference in the Fig. 8(a) and (b) is that in the region about the motor endplate in Fig. 8(a), the field is triphasic, but this is not apparent in the simulated SQUID scan. The triphasic behavior in the area of the motor endplate is due, most probably, to the various locations of the motor endplates on the multiple fibers in the motor unit. High-resolution magnetic scans could readily determine the spatial characteristics of the motor end plate zone.

C. The Far-Field Effect

Fig. 9 shows the arrival times of the peaks of the waveform along the length of the fiber, taken from the experimental and theoretical data just presented. The fiber endplate is located at 0.0 on the horizontal axis and the data points rising away from the origin show the propagation of the signal in both directions. As the signal propagates along the length of the fiber, the arrival time increases in proportion to the ratio of the distance

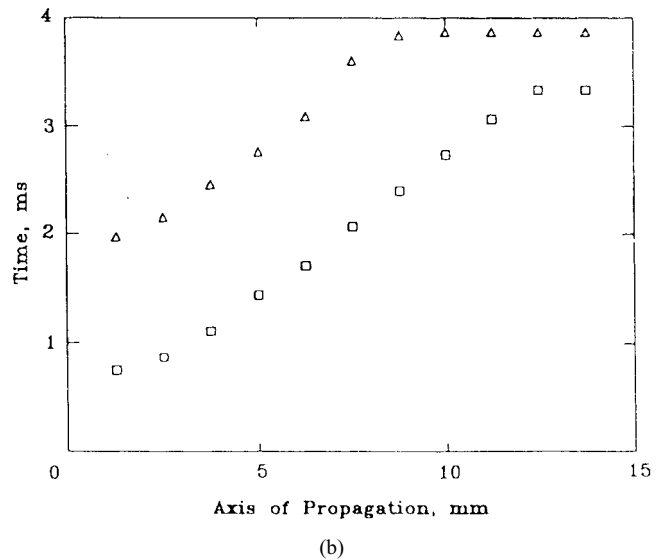
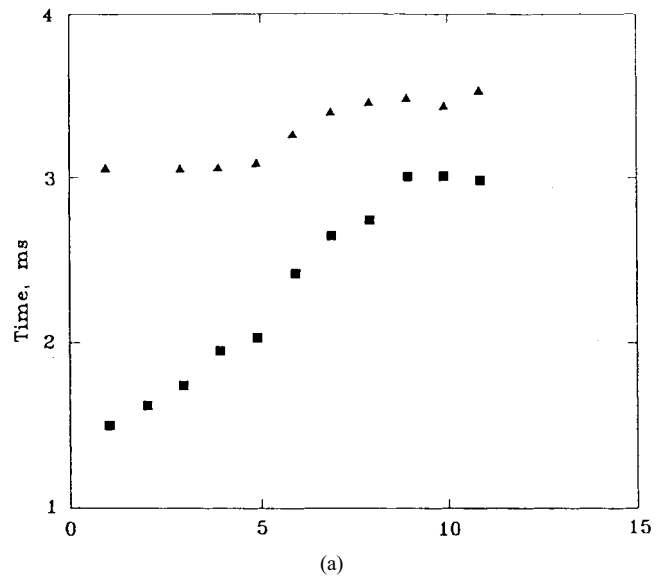


Fig. 9. Peak arrival times for (a) experimental data [16] and (b) simulated data. Squares denote arrival times of the first peak and triangles denote those of the second peak.

to the velocity of the signal. Fig. 9(a) shows the arrival times for the positive and negative peaks of the experimental data of Fig. 8(a). Fig. 9(b) shows the corresponding simulation from Fig. 8(b). In both experiment and simulation, when the graph goes flat at large z , the peak field measured beyond the length of the fiber occurs at the same point in time. The curve then has no slope and, hence, the peak appears to have an infinite velocity. This instantaneous propagation is known as a *far-field effect* [16], [17].

The simplicity of the propagating current-element model offers a simple explanation for the far-field effect; namely, the deconstruction of the action signal as the current elements collapse upon reaching the tendon at the end of the muscle fiber. This point is illustrated more clearly in Fig. 10. In the figure, magnetometer recordings were simulated at multiple locations separated by 1 mm along the length of a single muscle fiber and beyond, much like the toroid experiments

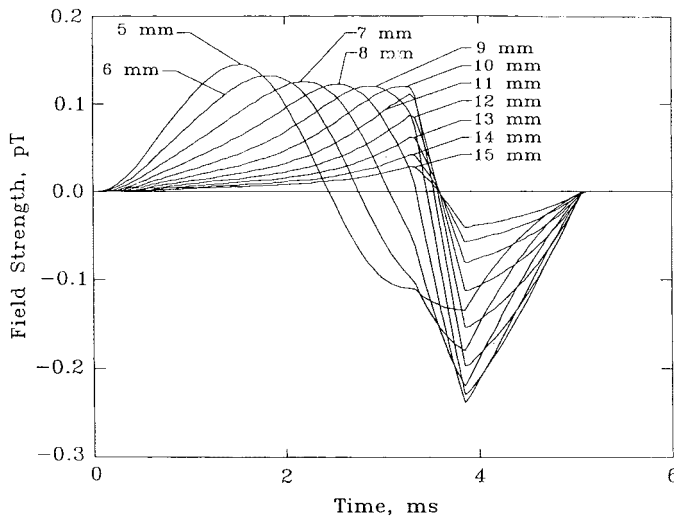


Fig. 10. Simulated scan along the length of a fiber and beyond with a SQUID pickup coil. The fiber is 10-mm long. The first measurement is taken at 5 mm downstream from the motor endplate region. The last five waveforms in the sequence are measured beyond the length of the fiber.

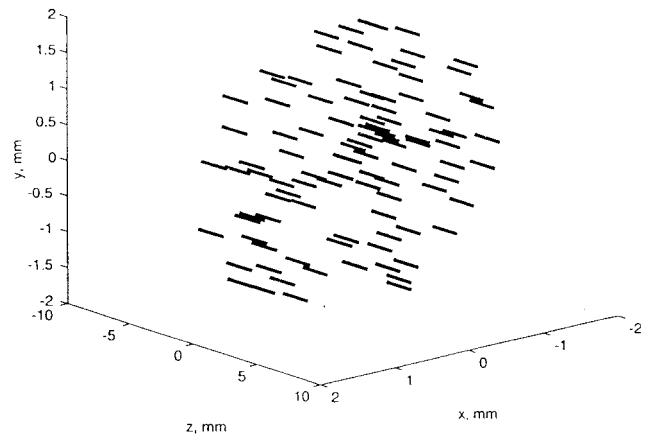
TABLE II
PARAMETER VALUES FOR THE CURRENT-ELEMENT
MODEL OF THE SMUCAF AS SIMULATED IN FIG. 11

Current in First Element	43.3 nA
Current in Second Element	-18.6 nA
Conduction Velocity	4.0 m/s
Fiber Length	20 mm
Number of Fibers	100
Endplate Width	0.6 mm
Appearance Times	1.0, 1.39, and 2.3 ms
Radius of Motor Unit	2.0 mm
Field Point	$x'=-2.0, y'=2.0, z'=0.0$ mm

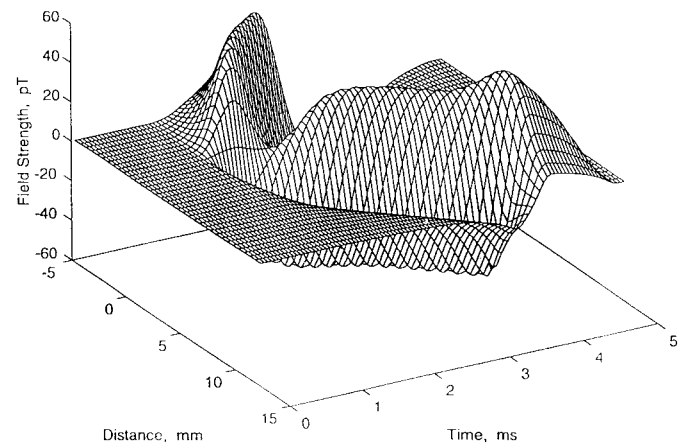
previously discussed. The fiber had a half-length of 10 mm and a conduction velocity of 3 mm/ms. In Fig. 10, the last five recordings were beyond the termination of the muscle fiber at the tendon. Each waveform represents a recording at a different location, z_s , along the z -axis. Just after 3 ms, the first current element of the pair has reached the tendon and has started to collapse. This is evident at the positive peak in the $z_s = 10$ -mm trace. The peaks thereafter represent the field measured beyond the end of the fiber. All of these peaks are occurring at the same point in time, thus, indicating that the signal has ceased propagation. The point in time at which these peaks occur corresponds to the arrival of the current-element pair at the tendon. The jagged shape of the waveform at that point is due to elimination of the first integral in (14) and the subsequent dominance of the second integral. All signals are extinguished by 5 ms.

D. Multiple Fiber Simulation

Table II shows the parameters for a simulation of a scanned measurement of the SMUCAF from a 100-fiber motor unit in the same fashion of the experimental and simulation results



(a)



(b)

Fig. 11. (a) The positions of the 100 fibers in the motor unit and the extents of their endplate widths. (b) The field strength as the magnetometer is scanned along the bundle in the same fashion as in Fig. 8.

presented in Fig. 8. The propagation velocity is now 4.0 m/s, whereas previously we had used a propagation velocity of 3.0 m/s. Times for launching the current elements have been changed, accordingly, to preserve the spatial extent of the AP as seen in the previous simulations. The fiber positions were selected randomly within a motor-unit radius of 2.0 mm. Endplate width was 0.6 mm and the center of the endplates were within ± 0.3 mm of the origin on the z -axis. Their distribution is also shown in Fig. 11. The results are similar to those of Fig. 8, but careful inspection yields that at $z = 0.0$, the AF is nonzero. This is a direct effect of the displacement of the endplates from $z = 0.0$, where there is no longer the perfect cancellation of the field that occurred when the AF was launched from symmetrical points on either side of the geometric center of the fibers, as was seen in the simulation result of Fig. 8. This simulation more closely resembles the experimental result from Fig. 8 if one discounts the effects of nonuniform propagation as shown in both Figs. 8 and 9.

VI. CONCLUSIONS

We have adapted a published model for the SMUCAP and extended it to predict the SMUCAF. We have discussed propagation rules for both models. We have validated the

SMUCAF model with extensive simulations and compared these results with both experimental and theoretical results of other researchers. The model is computationally efficient and has an analytical solution. The development of such a model should simplify the implementation of an inverse model to ascertain motor unit parameters from magnetic measurements of cellular AF's.

ACKNOWLEDGMENT

The authors wish to thank L. Li for assistance with preparing the figures. They would also like to thank Dr. N. Sepulveda for his comments on the derivations. Finally, they would like to thank the Living State Physics group for their collective comments on the manuscript.

REFERENCES

- [1] F. L. H. Gielen and J. P. Wikswo, Jr., "Electric and magnetic motor unit action signals in the rat," in *Proc. 38th Annu. Conf. Engineering in Medicine and Biology*, 1985, p. 340.
- [2] D. Cohen and E. Givler, "Magnetomyography: Magnetic fields around the human body produced by skeletal muscles," *Appl. Phys. Lett.* vol. 21, pp. 114–116, 1972.
- [3] F. L. H. Gielen, B. J. Roth, and J. P. Wikswo, Jr., "Capabilities of a toroid-amplifier system for magnetic measurement of current in biological tissue," *IEEE Trans. Biomed. Eng.* vol. BME-33, pp. 910–921, 1986.
- [4] D. B. MacHattie, "Investigation of the evoked magnetic action flux of skeletal muscle," Ph.D. dissertation, McMaster Univ., Hamilton, Ont., Canada, 1987.
- [5] S. J. Williamson and L. Kaufman, "Biomagnetism," *J. Magnetism, Magnetic Materials*, vol. 22, no. 2, pp. 129–202, 1981.
- [6] R. S. Wijesinghe, "A mathematical model for calculating the vector magnetic field of a single muscle fiber," *Math. Biosci.* vol. 208, pp. 208:53–55, 1991.
- [7] K. K. Parker and J. P. Wikswo, Jr., "Application of artificial neural networks to the biomagnetic inverse problem: Preliminary results," *Bull. Amer. Phys. Soc.*, vol. 37, p. 29, 1992.
- [8] K. K. Parker, "Forward and inverse modeling of the magnetic fields from single motor unit compound action potentials in skeletal muscle," Master's thesis, Vanderbilt Univ., Nashville, TN, 1993.
- [9] R. Plonsey, *Bioelectric Phenomena*. New York: McGraw-Hill, 1969.
- [10] J. D. Jackson, *Classical Electrodynamics*. New York: Wiley, 1975.
- [11] R. Plonsey and R. C. Barr, *Bioelectricity—A Quantitative Approach*. New York: McGraw-Hill, 1988.
- [12] K. C. McGill and A. Huynh, "Model of the surface-recorded motor-unit action potential," in *Proc. IEEE EMBS 10th Annu. Int. Conf.*, 1988, vol. 10, pp. 1697–1699.
- [13] K. C. McGill, personal communication, 1990.
- [14] J. M. van Egeraat, R. N. Friedman, and J. P. Wikswo, Jr., "The magnetic field of a single muscle fiber: First measurements and a core conductor model," *Biophys. J.*, vol. 57, pp. 663–667, 1990.
- [15] K. R. Swinney and J. P. Wikswo, Jr., "A calculation of the magnetic field of a nerve action potential," *Biophys. J.* vol. 32, pp. 719–732, 1980.
- [16] J. M. van Egeraat, "Magnetic aspects of nonuniform propagation of action signals in biological fibers," Ph.D. dissertation, Vanderbilt Univ., Nashville, TN, 1991.
- [17] D. G. Kline, E. R. Hackett, and P. R. May, "Evaluation of Nerve Injuries by Evoked Potentials and Electromyography," *J. Neurosurg.* vol. 31, pp. 128–136, 1969.

Kevin Kit Parker received the B.S. degree in biomedical engineering from Boston University, Boston, MA, in 1989 and the M.S. degree in mechanical engineering from Vanderbilt University, Nashville, TN, in 1993. His M.S. thesis was titled "Forward and Inverse Modeling of the Magnetic Fields from Single Motor Unit Compound Action Potentials in Skeletal Muscle." He is currently pursuing the Ph.D. degree in biological and applied physics at Vanderbilt University.

His research interests include bioelectromagnetoelastics, cellular engineering, and applications of artificial neural networks.



John P. Wikswo, Jr., (S'75–M'75) received the B.A. degree in physics from the University of Virginia, Charlottesville, in 1970, and the Ph.D. degree in physics from Stanford University, Stanford, CA, in 1975.

He was a Research Fellow in Cardiology at the Stanford University School of Medicine from 1975 to 1977, where he continued his work on determining the relationship of the electric and magnetic fields of the heart and developing instrumentation and analysis techniques for magnetocardiography. He then joined the faculty in the Department of Physics and Astronomy at Vanderbilt University, Nashville, TN, where he is now Professor of Physics and the A. B. Learned Professor of Living State Physics. His current research is directed toward using electric and magnetic measurements and electromagnetic theory for nondestructive testing and for studying the propagation of electrical activity in isolated cardiac tissue and in intestinal smooth muscle. He has published over 90 research articles and book chapters and more than 170 conference papers, abstracts, and reports. He holds nine patents.

Dr. Wikswo is a fellow of the American Physical Society.